Dalton Transactions

ROYAL SOCIETY OF CHEMISTRY

PAPER

View Article Online
View Journal | View Issue

Cite this: *Dalton Trans.*, 2025, **54**, 10761

In situ X-ray study of breathing-like effect in interlocked metal–organic nanocages†

Javier Martí-Rujas, * Stefano Elli and Antonino Famulari

Received 19th May 2025,
Accepted 13th June 2025

DOI: 10.1039/d5dt01186h

rsc.li/dalton

Using *in situ*-variable temperature single-crystal X-ray diffraction (VT-SCXRD) and solid-state quantum mechanical (QM) molecular modelling, the structural adaptability of mechanically interlocked $M_{12}L_8$ metal–organic cages (MOCs) including different guests is reported. Upon heating, the interlocked material shows a different response as a function of the guest's templating behavior, including a swelling and breathing-like effect of the $M_{12}L_8$ nanocages. The X-ray structures and solid-state QM calculations were used to analyse the energetic aspects related to the stability of the overall architectures. The energy of the 1D chains of interlocked $M_{12}L_8$ cages is investigated together with the stabilisation energy of $M_{12}L_8$ cages and $M_{12}L_8$ chains immersed in the crystalline phases. The role of the N–Zn–N coordination angles and the mechanical bonds in the breathing-like effect and the stability of the interlocked material is discussed.

Poly-[*n*]-catenanes (PCs) self-assembled from metal–organic cages (MOCs) linked by mechanical bonds (hereafter PCs-MOCs)[1] are a relatively new class of supramolecular materials. PCs-MOCs combine the characteristics of MOCs[2] and the properties of mechanically interlocked materials (MIMs).[3] Such polymeric MIMs have attracted scientific attention as their high densities of mechanical bonds are expected to unlock new mechanical, thermal and stimuli-responsive properties.[1c,4] PCs-MOCs are currently studied not only for their aesthetic aspects, but also because of their potential applications in gas adsorption,[5] electron conductivity, X-ray attenuation[6] and molecular recognition.[7] In such supramolecular structures, mechanical bonds play a crucial functional role, ranging from precise spatial organization to enhanced structural stability. Depending on the direction in which the mechanical bonds extend, PCs-MOCs can be one-dimensional (1D), two-dimensional (2D) or three-dimensional (3D) structures containing a high density of mechanical bonds. So far the reported PCs-MOCs are 1D or 3D[1] while 2D PCs-MOCs are yet to be discovered, although recently a mechanically interlocked 2D polymer[3g] not self-assembled from MOCs has been reported.

One class of PCs-MOCs is those self-assembled from large $M_{12}L_8$ nanocages.[8–10] The structures are formed from mechanically interlocked icosahedral $M_{12}L_8$ MOCs with internal volumes of *ca.* 2700 Å^3 (Scheme 1). Eight of the twenty triangular faces of the icosahedra are occupied by rigid triangular ligands, while the remaining twelve faces are free, giving rise to large windows. Due to the open surface of the $M_{12}L_8$ nanocages, they have been defined as *open icosahedra*.[11] Mechanical bonds are formed through the $M_{12}L_8$ windows and extend along the crystallographic *c*-axis forming 1D chains of connected MOCs. In the crystal lattice, after the packing of the 1D chains of $M_{12}L_8$ nanocages, the structure does not form channels but forms isolated voids, and some of the included

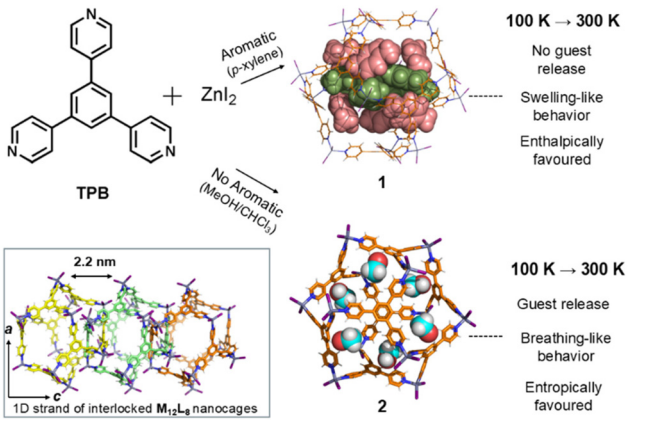

Scheme 1 Synthesis of **1** and **2** yielding $M_{12}L_8$ nanocages filled with ordered *p*-xy guests acting as templating agents in **1**, and in **2** where guest molecules are partially ordered with a poor templating effect. The inset shows the interlocking of three $M_{12}L_8$ nanocages propagating along the *c*-axis in which solvent molecules have been omitted for clarity purposes.

Dipartimento di Chimica Materiali e Ingegneria Chimica "Giulio Natta", Politecnico di Milano, Via L. Mancinelli 7, 20131 Milan, Italy. E-mail: javier.marti@polimi.it

† Electronic supplementary information (ESI) available. CCDC 2452216, 2452217, 2452221–2452223, 2452231–2452233 and 2452242. For ESI and crystallographic data in CIF or other electronic format see DOI: https://doi.org/10.1039/d5dt01186h

solvents (*i.e.*, aromatic) are retained over 15 days whilst preserving the structural features.[12] Because of the notable structural stability of $M_{12}L_8$ PCs-MOCs, guest exchange reactions can be carried out *via* multiple single-crystal-to-single-crystal (SCSC) reactions[7] which furnish aspects such as aromatic molecular recognition. However, if the guests are non-aromatic and small, they interact less efficiently with the walls of the $M_{12}L_8$ cages and are severely disordered. This lack of host–guest interactions can facilitate the guest's release from the cages as an entropically favoured process.[10a,13] Despite the host–guest chemistry carried out on $M_{12}L_8$ PCs-MOCs, additional structural and X-ray crystallographic analyses are needed to better understand aspects related to the guest templating effect, guest exchange, and evolution of the host sub-structure during the molecular replacement or release. Such information is crucial to obtain insights into whether certain chemical reactions and/or solid-state processes can be carried out in the interior of the nanostructured $M_{12}L_8$ cages, for instance, to understand if small gases like CO_2, CH_4 or N_2 can be trapped and/or stabilized in the $M_{12}L_8$ cavities by electrostatic interactions. Moreover, those aspects can furnish information regarding molecular transport/diffusion among interlocked $M_{12}L_8$ nanocages, as has been done in other organic 1D tunnel structures[14a–c] and metal–organic frameworks.[14d–f]

Here, using *in situ* VT-SCXRD and density functional theory (DFT) calculations, we have studied the structural evolution of the host and guest sub-structures at different temperatures in two crystals of $M_{12}L_8$ poly-[*n*]-catenanes including different guests. One crystal has $M_{12}L_8$ filled with ordered paraxylene (*p*-xy) (**1**) that is also subjected to a single-crystal-to-single-crystal (SCSC)[15] guest exchange. Meanwhile the second crystal (**2**) contains ordered methanol (only below 300 K) and disordered chloroform and/or methanol (Scheme 1). The current results help in understanding how the interlocked $M_{12}L_8$ cages change their void volume as a function of the guests at different temperatures. The $M_{12}L_8$ host structure shows a breathing-like effect that depends on the temperature and included guest molecules. The combined experimental XRD and DFT analyses provide insights into the structural information involved in the mechanisms behind the guest inclusion/exclusion in nanostructured interlocked MOCs. In particular, DFT calculations, specifically for the solid state (*i.e.*, to simplify the outcomes, solvent molecules have been removed), focusing on the interchain and the intrachain energies, are performed. The DFT results allow the rationalization of the stabilities correlated with $M_{12}L_8$ cages and the 1D chains of interlocked $M_{12}L_8$ cages in the crystalline architecture of poly-[*n*]-catenanes. The stabilities of **1** and **2** are strongly correlated with their unit cell volume (V_c) densities, with the smaller V_c being more stable. This work highlights the importance of the extended mechanical bonds in the stability of the 1D interlocked material, and the role of the N–Zn–N coordination bond angles in the breathing-like effect. PCs-MOCs[1c] have great potential due to the high density of mechanical bonds in polymeric structures and the structural voids that can be used as porous functional materials in the field of sensors, gas adsorption or actuators. As observed in other MIMs, a high density of mechanical bonds can give rise to unknown thermal,[16] mechanical,[17] and stimuli-responsive properties.[18] This is the first *in situ* structural analysis monitoring the $M_{12}L_8$ structural evolution as a function of temperature and guest content in this type of MIM.

Results and discussion

VT-SCXRD experiments were carried out using two single crystals self-assembled from interlocked icosahedral $M_{12}L_8$ nanocages. The first experiment was performed on a poly-[*n*]-catenane with $M_{12}L_8$ nanocages filled with *p*-xy guests (**1**) while the second crystal (**2**) contains methanol, partially filling the $M_{12}L_8$ cages (Scheme 1). In the *in situ* VT-SCXRD experiments, the temperature was gradually increased from 100 K to 300 K. Single crystals of **1** and **2** were grown using a triple-layering approach (Fig. S1 and S2†).[10a,b] Single crystals **1** and **2** were taken from the crystallization tube, immersed in mineral oil and, within 30 seconds, mounted on a loop and placed under a liquid N_2 flow. For the *in situ* VT-SCXRD experiments on **1** (Fig. 1) and **2**, five data sets were measured from 100 K to 300 K at intervals of 50 K, the lattice parameters monitored and their structures solved.

Structural evolution as a function of temperature of poly-[*n*]-catenane 1

The templating effect on the dynamic behavior of the $M_{12}L_8$ nanocages in **1** and **2** is evidenced by their different unit cell evolutions (Fig. 2). In **1**, the *a*/*b* lattice parameters increase

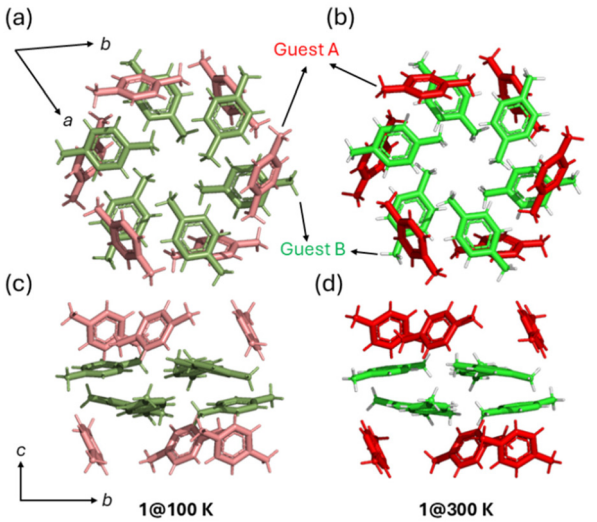

Fig. 1 SC-XRD guest-substructures in **1** at 100 K and 300 K. The $M_{12}L_8$ host sub-structure is not shown for clarity purposes. The efficient templating effect shown by the two *p*-xy molecules is evident as viewed along the [001] direction (a and b). View along the [100] direction (c and d). Guest A in red salmon color; guest B in dark green color for the structure at 100 K. Guest A in red color; guest B in green color for the structure at 300 K.

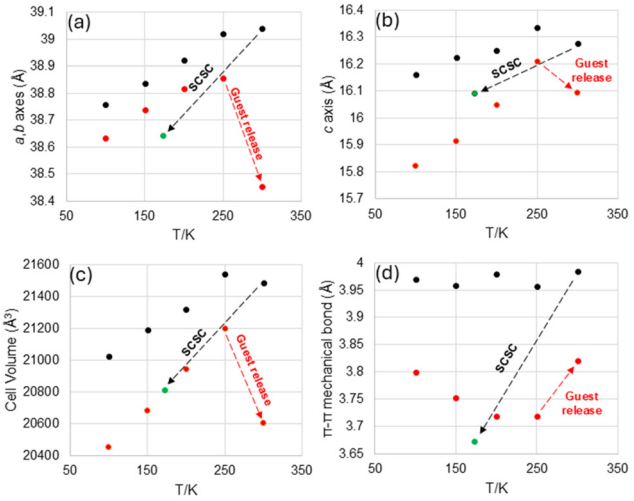

Fig. 2 Lattice parameter evolution from 100 K to 300 K in two single crystals containing *p*-xy (black dots) (**1**), and crystallized using nonaromatic solvents (chloroform and methanol) (red dots) (**2**). The green circle shows the lattice parameters of **1′** obtained after a guest exchange reaction *via* SCSC where *p*-xy is replaced by nitrobenzene (NB) in **1**. (a) Lattice *a*- and *b*-axes; (b) *c*-axis; (c) unit cell volume (V_c) and (d) TPB benzene–benzene distances.

from 100 K to 300 K, and the *c*-axis increases from 100 K to 250 K but experiences a small decrease upon reaching 300 K. The overall V_c variation in **1** in the 250–300 K interval is a decrease of ~50 Å^3 (Fig. 2c). The small compression is not because of solvent loss, as the SC-XRD data show that A and B *p*-xy molecules are in the asymmetric unit (Fig. S3†). The interpretation of this lattice evolution is that the shape of the $\mathbf{M_{12}L_8}$ cages did not suffer a significant change. This is explained by the templating *p*-xy guests not allowing much compression of the $M_{12}L_8$ nanocages due to the good interactions with the $M_{12}L_8$ host structure (*i.e.*, π–π contacts in a tight environment). The guest clusters in the cages in the X-ray structures at 100 K (**1@100 K**) and at 300 K (**1@300 K**) are shown in Fig. 1 to visualize the structural evolution of the host and guest sub-structures.

SC-XRD analysis of **1@100 K** resulted in the formula $[(ZnI_2)_{12}(TPB)_8]_{12}$(*p*-xy), with two ZnI_2, one TPB ligand, one-third of a second TPB in the host sub-structure and two independent (A and B) *p*-xy guest molecules in the guest sub-structure per asymmetric unit. The twelve *p*-xy guests included in one $M_{12}L_8$ nanocage can be observed along the *c*-axis (Fig. 1a and b). Viewed along the *a*-axis direction, guest A occupies the upper and lower poles of the $M_{12}L_8$ nanocages, while guest B is in the central area of the cage. In **1@300 K**, guests A and B remain in the cages with minor structural variations with respect to **1@100 K**. Fig. 1 depicts the two guest clusters showing that guests A and B occupy slightly different positions. In particular, Fig. 1c and d shows that guest B is a little more flattened or "squeezed" along the *c*-axis. However, the main information is that the structure is stable and the guest's templating effect is very important to fill the $M_{12}L_8$ voids.

Structural evolution as a function of temperature of poly-[*n*]-catenane 2

It is worth mentioning that large single crystals of $M_{12}L_8$ poly-[*n*]-catenanes have been grown *for the first time* using a mixture of small guest molecules, like chloroform and methanol, that are poor templating agents, as no host–guest aromatic–aromatic interactions are established.[7,10a,b,11,12] So far, all grown single crystals of $M_{12}L_8$ poly-[*n*]-catenanes have been obtained using aromatic guests to dissolve TPB and self-assemble it into MIMs. Therefore, in this case, there must be an important entropic/enthalpic contribution of the guest sub-structure in the self-assembly of **2** to form such large single crystals. SC-XRD analysis of **2@100 K** resulted in the formula $[(ZnI_2)_{12}(TPB)_8]_6$(MeOH), with two ZnI_2, one TPB ligand, and one-third of a second TPB as host sub-structure in the asymmetric unit. Only one methanol guest in the asymmetric unit (six per $M_{12}L_8$ cage) could be determined crystallographically in the 100–250 K range, whereas at 300 K, methanol was not localized. In **2**, the void space considering the methanol guest is 29% of the total unit cell volume.

In **2**, while from 100 K to 250 K, the behavior is similar to that of **1**, with an increase in the *a*/*b*/*c* lattice parameters, there is a significant decrease in the lattice vectors *a* and *b* (*i.e.*, 0.4 Å) from 250 K to 300 K. In this thermal range, the *c*-axis behaves as it does in the crystal containing *p*-xy (**1**) with a slight decrease. Contextualizing the current structural change in different interlocked cage systems, a more pronounced shrinkage was described by Clever and co-workers.[1a] The dynamic behavior was in a [2]-catenane of interlocked two pseudo-spherical M_2L_4 MOCs upon Cl^- uptake. In that case, the Pd···Pd cage axis changed from 24.4 Å to 23.6 Å (*i.e.*, 0.8 Å) in an allosteric fashion. Compared to **1**, in **2**, V_c undergoes a notable variation by decreasing by 600 Å^3. We note that in a SCSC guest exchange reaction starting with the same type of $M_{12}L_8$ PCs-MOCs, V_c was reduced by ~1350 Å^3 when *p*-xy was replaced by *o*-dichlorobenzene (*o*-DCB).[7] In such cases, the main lattice change is in the *c*-axis which is decreased by ~0.64 Å, but maintaining the interlocking π–π distance of 3.926 Å.[7]

SCSC and lattice evolution in poly-[*n*]-catenane 1: replacing *p*-xy with nitrobenzene (NB) in a gas–solid reaction

One way to gain more information about the dynamic behavior of **1@300 K** host's sub-structure upon external stimuli is by comparing the structural evolution after a gas–solid guest exchange reaction. The host–guest energy interaction ($E_{host-guest}$) determined by DFT shows that NB interacts more strongly with TPB (~44 kcal mol^{-1}) against the $E_{host-guest}$ of ~35 kcal mol^{-1} determined for *p*-xy.[7] After **1** was measured at 300 K, the same crystal was exposed in a closed chamber to vapours of NB at room temperature for 2 days. The NB exposed crystal (hereafter **1′**) was then mounted on a nylon loop for SC-XRD at 173 K.[7] The structural solution showed the guest exchange of *p*-xy by NB but only one NB guest (per asymmetric unit) could be localized by X-ray crystallography.[7] The NB interacts not with the pyridine but with the benzene rings of the

TPB. The new lattice parameters after the SCSC reaction are shown in Fig. 2d and in the ESI.† All distances, including the mechanical bond (π–π interactions, Table S4†), decreased with respect to **1**. Thus, the guest exchange process induces a change in the host sub-structure by strengthening the benzene–benzene interactions in the mechanical bonds. The guest exchange also demonstrates the stability of the poly-[*n*]-catenane structure by adapting the $M_{12}L_8$ void's volume to the presence of the new guests. The crystallinity of **1′** is very good as the guest inclusion happens in a system without channels over two days *via* a gas–solid interface.

Discussion of the dynamic host–guest behavior and high density of mechanical bonds

The structural response of **1** to heating can be explained by the presence of the two *p*-xy molecules with a high boiling point (411 K) at 300 K templating the structure without guest release. The main variation in the V_c, in the range 250–300 K, is that it decreases by ~50 Å^3. On the other hand, **2**, in the same temperature interval, behaves differently with a significant change in the *ab* lattice parameters, the direction orthogonal to the propagation of the *mechanical bonds*. This is due to the solvent release in **2** at 300 K that resulted in the overall V_c decrease of ~600 Å^3.

That is explained by the absence of host–guest aromatic–aromatic interactions within the $\mathbf{M_{12}L_8}$ nanocages, resulting in a poor templating effect from the guest sub-structure. Thus, chloroform/methanol molecules leave the $M_{12}L_8$ nanocages at ~300 K. Additionally, considering the small molecular dimensions of methanol/chloroform, they can escape the cages through the large $M_{12}L_8$ windows. This is also corroborated in the powders of $\mathbf{M_{12}L_8}$ poly-[*n*]-catenane (crystal size ~1–10 μm) that keep methanol for only a short time (10 min) at 300 K, following a *crystalline-to-amorphous* transformation under ambient conditions (Fig. S5†).[13] Moreover, the low boiling points of the guests (334 K and 338 K for chloroform and methanol, respectively) also contribute to the release from the cages at 300 K, and for this reason, the V_c decreased from 21 197 Å^3 to 20 608 Å^3. However, it is notable that in **2** the structure does not collapse at 300 K as it is maintained as a large single crystal during the X-ray measurement.

The presence of a high density of mechanical bonds propagating along the *c*-axis direction makes these crystallographic areas energetically stronger compared to regions dominated by weaker electrostatic contacts (with respect to *ab* lattice parameters). It has been calculated that for a crystal with a thickness of 0.2 mm, along the *c*-axis there are *ca*. 87 400 mechanical bonds.[1c] Therefore, it is crucial to monitor the evolution of the benzene–benzene interactions in the mechanical bond direction upon heating (Fig. 2d). In **1**, the distance between benzene rings is fairly constant during the heating (Fig. 2d). In **2**, the mechanical bond interactions differ from those in **1**, with a shortening of π–π interactions from 100 K to 250 K, and a minimal ring separation at 300 K (~0.1 Å). Hence, along the mechanical bond direction, *both* crystals, despite exhibiting slightly different behaviors, always maintain efficient aromatic–aromatic interactions.[7]

Structural analysis of $M_{12}L_8$ unit cell void volume variation upon temperature increase

Further understanding of the dynamic behavior of the isolated $M_{12}L_8$ nanocages was obtained by considering the variation in the unit cell void volume.[19] The calculated void volume corresponds to the $M_{12}L_8$ internal space occupied by the guests, and it is important to describe their templating effect. In **1**, the efficient templating of the *p*-xy guest sub-structure means that it is able to maintain the increasing trend of the cage's void. It is worth noting that with heating **1**, the solvent does not leave the cages (for the two molecules at 300 K by SC-XRD, see the ESI†). As shown in Fig. 3c, in general, the V_c variation increases until 300 K. This $M_{12}L_8$ V_c change is like a *swelling* process. Thermodynamically, in this case, the evolution of the voids is favoured from an enthalpic point of view as no release of the guest takes place and the electrostatic interactions are still good (in **1@300 K** py-centroid to *p*-xy-centroid is 4.152 Å, Table S6†). In this regard, DFT calculations have also revealed that the host–guest interactions for molecules such as NB and *p*-xy are important with values from 44 to 25 kcal mol^{-1}, thus explaining the observed stability.[7]

Conversely, **2**, upon heating, shows a different trend in the cage volume. It starts with a sharp increase in the void volume, as the guests increase their dynamic behavior, but at *ca*. 250 K,

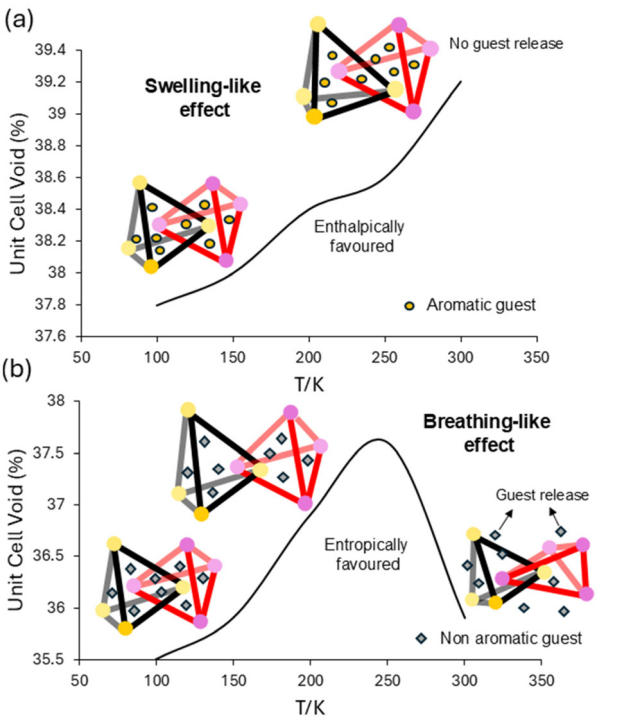

Fig. 3 Plot showing the evolution of the unit cell voids as a function of temperature. (a) Evolution of **1** including ordered *p*-xy without guest release following a "*swelling*" effect. (b) Plot showing the evolution of **2** upon heating. The poor templating effect of disordered and nonaromatic solvents (*i.e.*, methanol/chloroform) results in a "*breathing effect*" of the interlocked $M_{12}L_8$ cages. For clarity purposes, the cages are shown as interlocked tetrahedra.

the void volume shows an abrupt decrease and returns to a similar volume to that observed at 100 K. Our interpretation is that after **2** is frozen (100 K), and the included guests interact with each other more, the disorder is reduced. However, upon heating, the solvents move more, increasing the $M_{12}L_8$ cage volume (*i.e.*, the fraction of the cell volume occupied by the solvent is higher). Upon reaching 250 K, the disorder increases and the cages swell to a maximum, and then the solvent leaves the $M_{12}L_8$ cages, inducing a decrease in the cage's void volume at 300 K, as shown in Fig. 3b. This void decrease is mainly due to the *a*/*b* contraction. This process is like a *breathing* effect and is entropically favoured, which is also corroborated by SC-XRD data, as the crystallographic analysis does not resolve the methanol guest in the $M_{12}L_8$ nanocages as methanol has escaped the cages (Fig. 3b).[20]

Combined X-ray data and DFT calculations

The V_c decrease in **2** is mainly due to the shortening of the *a*/*b* lattice parameters, and the crystallographic directions along which the 1D chains of interlocked $M_{12}L_8$ MOC_S interact *via* C–H···I contacts (weaker electrostatic interactions). Along the *c*-axis, there are mechanical bonds which are energetically stronger. Thus, from an electrostatic point of view, in **1** and **2**, some crystallographic directions are stronger than others and explain the observed anisotropic dynamic response to external stimuli. Hence, in part, the dynamic behavior of the interlocked $M_{12}L_8$ nanocages depends on the *templating* guests and whether they interact efficiently with the host framework or not.

In this regard, QM calculations specific to solid-state systems are very important to gain host–host and host–guest structure–energy correlations.[10] DFT calculations on the isostructural TPB-$ZnBr_2$ poly-[*n*]-catenane demonstrated that the interactions among neighbouring chains are one order of magnitude weaker than the *mechanical bond* interactions.[12] The interactions among interlocked $M_{12}L_8$ cages in 1D porous rods are ~145 kcal mol^{-1}. On the "weaker" part of the MIM, the electrostatic interactions among non-interlocked $M_{12}L_8$ cages in the 1D chains are ~45 kcal mol^{-1}, which is comparable to the host–guest electrostatic interactions. In the present case, the DFT interaction energies among cages and among 1D chains, together with lattice energies, have been investigated for **2@300 K** and **1@300 K**. The DFT calculations, as in previous studies, have been performed at the PBE/DNP level (where PBE is the Perdew–Burke–Ernzerhof functional while DNP indicates the standard numerical basis set implemented in the Dmol^3 package[21] and roughly comparable to the 6-31G** Gaussian set). The adopted strategy showed good performances in some studies on crystalline systems (including molecules, polymers, and hybrid metal–organic materials).[22] An explicit van der Waals contribution, according to the approach proposed by Grimme, was determined.[23] We considered the "*interaction energies*" (E) among interlocked and noninterlocked nanocages, and the "*lattice energy*" (E^*) corresponding to the stabilisation of one single $M_{12}L_8$ cage or a 1D chain of interlocked cages *immersed* in the crystalline lattices.

E can be approximated by the interaction energies of two closely interacting dimers: two interlocked cages or two first non-mechanically linked neighbouring cages. The interaction energies considering the interlocked cages are 94.5 kcal mol^{-1} (that is almost 189 kcal mol^{-1} per 2 cages) and 64.7 kcal mol^{-1} (that is almost 129 kcal mol^{-1} per 2 cages) in the case of compounds **2@300 K** and **1@300 K** respectively. These interactions are quite high as they are influenced by the aromatic rings (π–π interactions) due to the mechanical bonds. The interaction energies among the non-interlocked cages are lower (*i.e.*, 46.8 kcal mol^{-1} and 33.6 kcal mol^{-1}) for **2@300 K** and **1@300 K**, respectively. These lower E values are explained by the electrostatic van der Waals interactions among the neighbouring $M_{12}L_8$ cages.

The average lattice energies E^* required to extract a single $M_{12}L_8$ cage immersed in the crystalline structure are very high, reflecting the great stability of the structures: about 503 kcal mol^{-1} and 357 kcal mol^{-1} for compounds **2@300 K** and **1@300 K**, respectively. The good stability is confirmed by the energy required to ideally remove a single infinite chain of interlocked cages from the crystalline structures: 400 kcal mol^{-1} and 306 kcal mol^{-1} for compounds **2@300 K** and **1@300 K**, respectively. These values are consistent with the energy interactions determined in the $ZnCl_2$ isostructural $M_{12}L_8$ poly-[*n*]-catenane.[10a]

The calculation results demonstrate three main conclusions: (i) the model of an infinite 1D chain packed into the crystalline architecture is a good model to explain the high stability of the materials under study; (ii) the stabilities are strongly correlated to densities of the materials being **2@300 K** denser (smaller V_c) with respect to **1@300 K** (larger V_c); and (iii) the structures remain stable while breathing (shrinking or swelling) under thermal treatments because the stabilization is preserved under variation of the V_c by the presence of the mechanical bonds.

From a host–guest electrostatic potential point of view, the mapped electrostatic potential (MEP) surfaces of TPB and *p*-xy guest molecules show that both can orient in such a way that the more positive surface of TPB can interact with the more negative area of the guest (Fig. 4). This complementary electrostatic potential surface allows good packing in **1** and increases the stability of the host–guest system. The centroid–centroid distances among *p*-xy and pyridine of the TPB ligand show only a small decrease upon heating, indicating (*i.e.*, from 100 K to 300 K) the good stability between the host and guest sub-structures (Fig. 4c).

Breathing-like effect, N–Zn–N coordination bond variations upon heating and guest inclusion in interlocked $M_{12}L_8$ nanocages

Hiraoka and co-workers demonstrated, through detailed geometric analyses of MOCs involving the N–Pd–N coordination bond angles in TPB, the *cis*-protected Pd(II) end-capping groups, and the ligand's pyridine and benzene ring dihedral angle control, that small angle variations are crucial for controlling their self-assembly.[24] Also remote geometric communi-

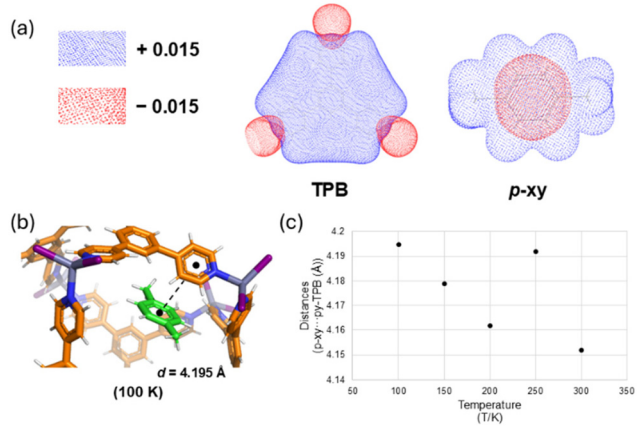

Fig. 4 (a) Plot of the MEPs of TPB and *p*-xy. (b) SC-XRD structure of **1@100 K** showing the distances among host and *p*-xy guest (guest A). (c) Graph with the evolution of the host–guest distances as a function of temperature.

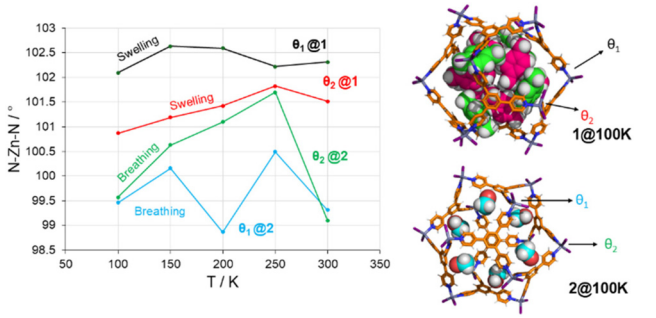

Fig. 5 (a) Plot showing the evolution of the two different coordination angles N–Zn–N as a function of temperature in the $M_{12}L_8$ cages for **1@100 K** and **2@100 K**. The measured θ_1 and θ_2 angles in the $M_{12}L_8$ nanocages are shown on the right side.

cations among neighbouring TPB ligands can give certain dynamic motion in $[M_{12}L_8]^{24+}$ icosahedral cages.[24] In the search for large spherical MOCs, Fujita and co-workers reported that the bend angle of arc-shaped ligands dictates the outcome product in the self-assembly of very large $M_{30}L_{60}$ cages, and very small changes (~3°) in such angles can yield markedly different products.[25]

In MOCs with internal voids of 2700 Å^3 formed of open icosahedra using flat TPB ligands and Zn(II) metals (**1** and **2**), the dynamic motion in coordination bonds and ligand torsional angles are necessary to allow guest exchange. In **2**, at *ca*. 250 K, the non-aromatic guests are released *via* the large windows of the $M_{12}L_8$ cages, and the *a*/*b*-axis shrinks because those are the weaker interactions among neighbouring 1D chains of interlocked MOCs. The packing of 1D chains of interlocked $M_{12}L_8$ MOCs yields a structure that does not have continuous channels but has isolated voids. Knowing that the TPB pyridine rings possess a discrete range of almost free rotation (*i.e.*, 3 kcal mol^{-1} at τ = 90°; with τ being the dihedral angle between the pyridine and benzene rings), behaving like a rotor, with τ = 36°,[7] we hypothesize that at 250 K, the local dynamic behavior of the pyridines (*i.e.*, rotation) in the $M_{12}L_8$ cages can create gates. Therefore, if many cages are connected by gates, transient channels can be formed allowing guests to diffuse to neighbouring cages until they reach the crystal surface. The transient channels are formed due to the local dynamic behavior of the pyridines and the structural strength of the mechanical bonds, that in a concerted manner with many pyridines rotating, allow the diffusion of guests within the structure as determined by multiple SCSC guest exchange reactions.[7] Thus, when the guest $M_{12}L_8$ content is low, the cages reduce the volume but still remain stable as determined by QM calculations. This is an entropically favoured process. We recall this process as a "*breathing*" effect by the $M_{12}L_8$ nanocages as shown in Fig. 3b.

The geometrical analysis of the icosahedron's N–Zn–N coordination bonds in **1** and **2** (*i.e.*, the icosahedron's vertices) upon heating is shown in Fig. 5. The plot demonstrates that the $M_{12}L_8$ cages of **2**, without aromatic solvents, show the breathing effect as the θ_1 angle increases up to 250 K but then decreases at 300 K as a result of the cage compression. The change in θ_2 is from 99.57° (100 K) to a maximum value of 101.7° (250 K), which changes to 99.10° (300 K) (Fig. 5). Thus, θ_1 and θ_2 increase by 1.03° and 2.13° respectively in the 100–250 K interval. Moreover, from 100 K to 300 K both θ_1 and θ_2 have decreased (Fig. 5). On the other hand, **1** shows a small increase in the N–Zn–N coordination bond angles from 100 K to 300 K, reflecting that the swelling effect is also influenced by the presence of *p*-xy guest molecules (Fig. 5).

Clearly, the N–Zn–N coordination angles play a crucial role in the $M_{12}L_8$ swelling and breathing effects. Considering that the Zn atoms are at the vertices of the icosahedron and that TPB ligands are rigid panels filling the eight icosahedral triangular faces, the open $M_{12}L_8$ icosahedra can respond in a dynamic manner to external stimuli, such as temperature and/or molecules by varying the coordination bond angles. Thus, in **1** and **2**, both the mechanical bonds (mechanical strength) and the N–Zn–N coordination bond angles (dynamic response to external stimuli) are crucial to explain the observed $M_{12}L_8$ breathing and swelling behavior. We believe that the above-mentioned aspects are relevant factors, acting in a concerted manner, and these contribute to understanding the guest uptake/exchange in $M_{12}L_8$ interlocked nanocages with large isolated voids, and not connected channels.[26]

Conclusions

Topologically 1D interlocked $M_{12}L_8$ MOCs, **1** and **2**, hosting different guests, have been studied by means of VT-SCXRD to monitor the dynamic behavior of the $M_{12}L_8$ host and guest sub-structures upon heating (100 K–300 K). Without aromatic guests (**1**), the $M_{12}L_8$ show a *breathing*-like effect due to the adaptable behavior of the host sub-structure upon heating and guest release. In both crystals (**1** and **2**), the mechanical bonds

remain stable through the external stimuli. The experimental results, supported by QM calculations specific for solid-state systems, demonstrate that energetically, the mechanical bond interactions are one order of magnitude higher than the inter-chain interactions and, in part, explain the different behavior of the $M_{12}L_8$ nanocages with the guest templating effect. Moreover, even if thermal treatments affect the V_c, the high stability is preserved due to the structural topology of the materials. The geometrical changes at the icosahedral vertices (N–Zn–N coordination angles) showed a higher variation in the absence of efficient templating guests. The angular variations in the coordination bonds, with concerted dynamic rotations of the TPB ligands, help rationalize the breathing effect and the guest inclusion/exchange reactions in structures not having connected channels but voids. The discovery of new materials with intriguing topologies and dynamic behavior upon external stimuli can serve well-characterized model systems for studying molecular transport/diffusion in nanostructured materials like actuators[27] in a controlled guest release.[28] Scientific progress in $M_{12}L_8$ poly-[*n*]-catenanes depends on the degree of knowledge of their chemical, physical and structural properties, which are crucial for their application in various fields of nanotechnology.

Conflicts of interest

There are no conflicts to declare.

Data availability

Crystallographic data for **1** and **2** at different temperatures have been deposited in the CCDC database under **1@100 K:** 2452216, **1@150 K:** 2452217, **1@200 K:** 2452221, **1@250 K:** 2452222, **1@300 K:** 2452242; and **2@100 K**, 2452223, **2@150 K:** 2452231, **2@200 K:** 2452232, **2@250 K:** 2452233 accession numbers and can be obtained from **https://www.ccdc.cam.ac.uk/structures/**.†

Data for **2@300 K** are available upon request from the author.

Acknowledgements

J. M.-R. thanks Politecnico di Milano for funding (Fondo Chiamata Diretta Internazionalizzazione. Prg. Id. 61566). A. F. and J. M.-R. acknowledge PRIN Project "SCINTILLA" (code number 2022SCWMT2). The authors acknowledge the NeXt GAME Laboratory at Politecnico di Milano where **1** and **2** VT-SCXRD data were recorded and analyzed.

References

1 (*a*) S. Freye, J. Hey, A. Torras-Galán, D. Stalke, R. Herbst-Irmer, M. John and G. H. Clever, *Angew. Chem., Int. Ed.*, 2012, **51**, 2191–2194; (*b*) Q.-Y. Hong, B. Huang, M.-X. Wu, J.-Y. Jiang, H.-B. Yang, X.-L. Zhao, G. H. Clever and X. Shi, *Nat. Commun.*, 2025, **16**, 2484–2496; (*c*) J. Martí-Rujas and A. Famulari, *Angew. Chem., Int. Ed.*, 2024, **63**, e202407626; (*d*) J. Martí-Rujas, *Commun. Chem.*, 2025, **8**, 92–109.

2 (*a*) M. Fujita, *Acc. Chem. Res.*, 2005, **38**(4), 369–378; (*b*) A. Mishra, A. Dubey, J. W. Min, H. Kim, P. J. Stang and K.-W. Chi, *Chem. Commun.*, 2014, **50**, 7542–7544; (*c*) R. A. Bilbeisi, T. K. Ronson and J. R. Nitschke, *Angew. Chem., Int. Ed.*, 2013, **52**, 9027–9030; (*d*) J. Martí-Rujas, *Mater. Adv.*, 2023, **4**, 4333–4343; (*e*) C. J. T. Cox, J. Hale, P. Molinska and J. E. M. Lewis, *Chem. Soc. Rev.*, 2024, **53**, 10380–10408; (*f*) W. He, Y. Yu, K. Iizuka, H. Takezawa and M. Fujita, *Nat. Chem.*, 2025, **17**, 653–662; (*g*) U. Kai, R. Sumida, Y. Tanaka and M. Yoshizawa, *J. Am. Chem. Soc.*, 2025, **147**, 10640–10646; (*h*) H. Xu, T. K. Ronson, A. W. Heard, P. C. P. Teeuwen, L. Schneider, P. Pracht, J. D. Thoburn, D. J. Wales and J. R. Nitschke, *Nat. Chem.*, 2025, **17**, 289–296.

3 (*a*) J. F. Stoddart, *Chem. Soc. Rev.*, 2009, **38**, 1802; (*b*) C. J. Bruns and J. F. Stoddart, An Introduction to the Mechanical Bond, in *The Nature of the Mechanical Bond: From Molecules to Machines*, John Wiley & Sons, Inc., Hoboken, NJ, 2016, pp. 3–54; (*c*) Z. Ashbridge, S. D. P. Fielden, D. A. Leigh, L. Pirvu, F. Schaufelberger and L. Zhang, *Chem. Soc. Rev.*, 2022, **51**, 7779–7809; (*d*) S. Mena-Hernando and E. M. Perez, *Chem. Soc. Rev.*, 2019, **48**, 5016–5032; (*e*) J. R. J. Maynard and S. M. Goldup, *Chem*, 2020, **6**, 1914–1932; (*f*) L. F. Hart, J. E. Hertzog, P. M. Rausher, B. W. Rawe, M. M. Tranquilli and S. J. Rowan, *Nat. Rev. Mater.*, 2021, **6**, 508–530; (*g*) M. I. Bardot, C. W. Weyhrich, Z. Shi, M. Traxler, C. L. Stern, J. Cui, D. A. Muller, M. L. Becker and W. R. Dichtel, *Science*, 2025, **387**, 264–269; (*h*) Z.-B. Tang, L. Bian, X. Miao, H. Gao, L. Liu, Q. Jiang, D. Shen, L. Xu, A. C.-H. Sue, X. Zheng and Z. Liu, *Nat. Synth.*, 2025, DOI: **10.1038/s44160-025-00791-x**.

4 (*a*) X. Kuang, X. Wu, R. Yu, J. P. Donahue, J. Huang and C.-Z. Lu, *Nat. Chem.*, 2010, **2**, 461; (*b*) L. Chen, Q. Chen, M. Wu, F. Jiang and M. Hong, *Acc. Chem. Res.*, 2015, **48**, 201–210; (*c*) M. P. Snelgrove, N. N. Sergeeva and M. J. Hardie, *Chem. – Eur. J.*, 2025, **31**, e202403692.

5 L. Jiang, P. Ju, X.-R. Meng, X.-J. Kuang and T.-B. Lu, *Sci. Rep.*, 2012, **2**, 668–673.

6 L. Cheng, C. Liang, W. Liu, Y. Wang, B. Chen, H. Zhang, Y. Wang, Z. Chai and S. Wang, *J. Am. Chem. Soc.*, 2020, **142**, 16218–16222.

7 J. Martí-Rujas, S. Elli, A. Zanotti, A. Famulari and F. Castiglione, *Chem. – Eur. J.*, 2023, **29**, e202302025.

8 J. Heine, J. Schmedt auf der Gunne and S. Dehnen, *J. Am. Chem. Soc.*, 2011, **133**, 10018.

9 E. C. Constable, G. Zhang, C. E. Housecroft and J. A. Zampese, *CrystEngComm*, 2011, **13**, 6864–6870.

10 (*a*) S. Torresi, S. Famulari and J. Martí-Rujas, *J. Am. Chem. Soc.*, 2020, **142**, 9537; (*b*) J. Martí-Rujas, S. Elli and A. Famulari, *Sci. Rep.*, 2023, **13**, 5605; (*c*) S. Elli, A. Famulari and J. Martí-Rujas, *ChemPlusChem*, 2024, **89**, e202400332.

11 J. Martí-Rujas, S. Ma and A. Famulari, *Inorg. Chem.*, 2022, **61**, 10863–10871.
12 J. Martí-Rujas and A. Famulari, *Cryst. Growth Des.*, 2022, **22**, 4494–4502.
13 (*a*) J. Martí-Rujas, S. Elli, A. Sacchetti and C. Castiglione, *Dalton Trans.*, 2022, **51**, 53–58.
14 (*a*) J. Marti-Rujas, A. Desmedt, K. D. M. Harris and F. Guillaume, *J. Am. Chem. Soc.*, 2004, **126**, 11124; (*b*) J. Martí-Rujas, A. Desmedt, K. D. M. Harris and F. Guillaume, *J. Phys. Chem. B*, 2007, **111**, 12339; (*c*) J. Martí-Rujas, A. Desmedt, K. D. M. Harris and F. Guillaume, *J. Phys. Chem. C*, 2009, **113**, 736–743; (*d*) B. A. Johnson, A. M. Beiler, B. D. McCarthy and S. Ott, *J. Am. Chem. Soc.*, 2020, **142**(28), 11941–11956; (*e*) C. H. Sharp, B. C. Bukowski, H. Li, E. M. Johnson, S. Ilic, A. J. Morris, D. Gersappe, R. Q. Snurr and J. R. Morris, *Chem. Soc. Rev.*, 2021, **50**, 11530–11558; (*f*) T. Maity, P. Malik, S. Bawari, S. Ghosh, J. Mondal and R. Haldar, *Nat. Commun.*, 2023, **14**, 2212–2229.
15 (*a*) M. Kawano and M. Fujita, *Coord. Chem. Rev.*, 2007, **251**, 2592; (*b*) Y. Zheng, X. Jia, K. Li, J. Xu and X.-H. Bu, *Adv. Energy Mater.*, 2022, **12**, 2100324; (*c*) K. Biradha and M. Fujita, *Angew. Chem., Int. Ed.*, 2002, **41**, 3392–3395; (*d*) Y. Wada, P. M. Usov, B. Chan, M. Mukaida, K. Ohmori, Y. Ando, H. Fuwa, H. Ohtsu and M. Kawano, *Nat. Commun.*, 2024, **15**, 81–88.
16 Q. Wu, P. M. Rauscher, X. Lang, R. L. Wojtecki, J. J. de Pablo, M. J. A. Hore and S. J. Rowan, *Science*, 2017, **358**, 1434.
17 Z. Zhang, J. Zhao and X. Yan, *Acc. Chem. Res.*, 2024, **57**, 992–1006.
18 Y. Noda, Y. Hayashi and K. Ito, *J. Appl. Polym. Sci.*, 2014, **131**, 40509.
19 The void volumes for **1** and **2** have been determined by manually removing the guest molecules from the CIF files. To determine the void volume variation, the unit cell voids have been calculated using a spherical probe with a radius of 1.2 Å using Mercury program (version 2022.1.0). L. J. Barbour, *Chem. Commun.*, 2006, 1163. For **2**, the accuracy of the void calculation is not affected by whether a guest is ordered or disordered. Since the guests are included within the cages, the void calculation takes into account the space that guests are occuppying in the $M_{12}L_8$ internal space as the $M_{12}L_8$ sub-structure is well characterized by SC-XRD.
20 We note that the *R*-factors in the 2@300K (Table S18†) structure have worsened compared to 2@250K (Table S17†). This is explained by the gradually weaker diffraction which is also induced by the methanol guest release at 300 K.
21 J. P. Perdew, K. Burke and M. E. Ernzerhof, *Phys. Rev. Lett.*, 1996, **77**, 3865–3868.
22 (*a*) L. Catalano, D. P. Karothu, S. Schramm, E. Ahmed, R. Rezgui, T. J. Barber, A. Famulari and P. Naumov, *Angew. Chem., Int. Ed.*, 2018, **57**, 17254–17258; (*b*) A. Famulari, G. Raos, A. Baggioli, M. Casalegno, R. Po and S. V. Meille, *J. Phys. Chem. B*, 2012, **116**, 14504–14509; (*c*) J. Martí-Rujas and F. Guo, *Dalton Trans.*, 2021, **50**, 11665–11680.
23 (*a*) S. Grimme, *J. Chem. Phys.*, 2006, **124**, 34108–34124; (*b*) A. Baggioli, S. V. Meille, G. Raos, R. Po, M. Brinkmann and A. Famulari, *Int. J. Quantum Chem.*, 2013, **113**, 2154–2162; (*c*) A. Baggioli and A. Famulari, *Phys. Chem. Chem. Phys.*, 2014, **16**, 3983–3994.
24 T. Abe, K. Takeuchi, M. Higashi, H. Sato and S. Hiraoka, *Nat. Commun.*, 2024, **15**, 7630–7646.
25 D. Fujita, Y. Ueda, S. Sato, N. Mizuno, T. Kumasaka and M. Fujita, *Nature*, 2016, **540**, 563–566.
26 The variations in distances and angles described in **1** and **2** are "small" in order to sustain the structural transformations whilst maintaining the single crystallinity (*i.e.*, SCSC transformations). If these structural variations are more pronounced the single crystallinity will not be preserved. In **1**, multiple SCSC can be performed at room temperature[7] because there is a concerted dynamic behavior involving variations in lattice cell parameters, dihedral angles and coordination bond angles upon external stimuli (*i.e.*, guest molecules and temperature).
27 L.-L. Dang, J. Zheng, J.-Z. Zhang, T. Chen, Y.-H. Chai, H.-R. Fu, F. Aznarez, S.-R. Liu, D.-S. Li and L.-F. Ma, *Angew. Chem., Int. Ed.*, 2024, **63**, e202406552.
28 W. Meng, S. Kondo, T. Ito, K. Komatsu, J. Pirillo, Y. Hijikata, Y. Ikuhara, T. Aida and H. Sato, *Nature*, 2021, **598**, 298–303.

